Deliverable D4.1
Thermomechanical characterization of refractory microstructures finished

Document type	**Deliverable D 4.1**
Document Version / Status	**2.0**
Primary Authors	**Dietmar Gruber, dietmar.gruber@unileoben.ac.at, MUL**
Distribution Level	**PU (Public)**
Project Acronym	**ATHOR**
Project Title	**Advanced THermomechanical multiscale mOdelling of Refractory linings**
Grant Agreement Number	**764987**
Project Website	www.etn-athor.eu
Project Coordinator	**Marc Huger, marc.huger@unilim.fr, UNILIM**
Document Contributors	**Marc Huger, marc.huger@unilim.fr, UNILIM** **Dietmar Gruber, dietmar.gruber@unileoben.ac.at, MUL** **Thanh Hung Nguyen, thanh.nguyen@unileoben.ac.at, MUL** **Farid Asadi, farid.asadi@unilim.fr, UNILIM** **Glyn Derrick, glyn.derrick@unilim.fr, UNILIM**

History of Changes

Version	Date	Author (Organization)	Change	Page
1.0	22.06.2020	Hung Nguyen (MUL)	Introduction, device description, results for alumina spinel and magnesia spinel bricks	2 to 7
1.1	28.06.2020	Farid ASADI (UNILIM)	Section 5 & Conclusion	7 to last
1.2	29.06.2020	Glyn Derrick (UNILIM)	Formatting and English check	All
1.3	01.07.2020	Hung Nguyen (MUL)	Section 3, 4 and 6	2,3,4,5,7,13
1.4	02.07.2020	Glyn Derrick (UNILIM)	Formatting and English check	All
1.5	05.07.2020	Farid ASADI(UNILIM) Hung Nguyen(MUL) Glyn Derrick(UNILIM)	Final corrections	All
1.6	06.07.2020	Dietmar Gruber(MUL)	Final corrections	All
1.7	21.07.2020	Marc Huger (UNILIM)	Proofreading	All
1.8	24.07.2020	Hung Nguyen (MUL)	Add results from MWST with SEM	9,10,11,16
1.9	05.08.2020	Dietmar Gruber(MUL)	Final corrections	All
2.0	25.08.2020	Marc Huger (UNILIM)	Minor corrections and final validation	All

European Commission
Horizon 2020
European Union funding
for Research & Innovation

1 Introduction

This report will review the fracture evolution depending on the microstructure of samples during loading observed by optical microscopy or SEM using two dedicated devices developed at UNILIM and MUL. This will support DEM results from WP3 and will help to build a better understanding of the relationship between a intentional, pre-established micro-cracks network generated by CTE (Coefficient of Thermal Expansion) mismatch between different constituents and the ability of the material to develop a R-Curve behaviour. The miniaturized wedge splitting test was developed for this purpose. The dimensions of the device allow direct observation of the crack propagation with both optical microscopes and SEM. Tests were performed on samples made from alumina spinel bricks, magnesia spinel bricks and alumina spinel model refractory castables. The results obtained from these experiments will serve as a benchmark for future simulation.

2 Miniaturized wedge splitting device

The wedge splitting test [1] [2] has been the standard method for fracture testing of refractory materials since 1986, when it was first introduced by Tschegg. A notched specimen, resting on a linear support, is subjected to a vertical force, which is transformed to a higher horizontal force via load transmission equipment (wedge, rollers, load transmission pieces) situated in a groove of the

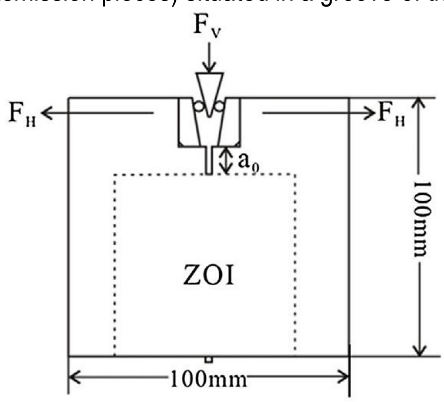

specimen (Figure 1).

European Commission
Horizon 2020 European Union funding for Research & Innovation

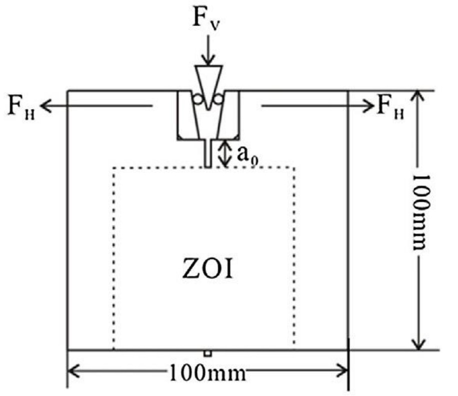

Figure 1: Schematic representation of wedge splitting specimen shape [3].

The applied load and displacement are then monitored throughout the experiment. Direct observation of the fracture with SEM, would result in a better understanding of the micro-fracture mechanism. Unfortunately, the size of the wedge splitting test impedes such direct observation, it is for this reason, the miniaturized wedge splitting test was developed.

2.1 Device developped at MUL

The miniaturized wedge splitting test device in MUL is 200mm long, 100mm wide and 90mm high. This allows for direct observation of the fracture under optical microscopes and SEM (

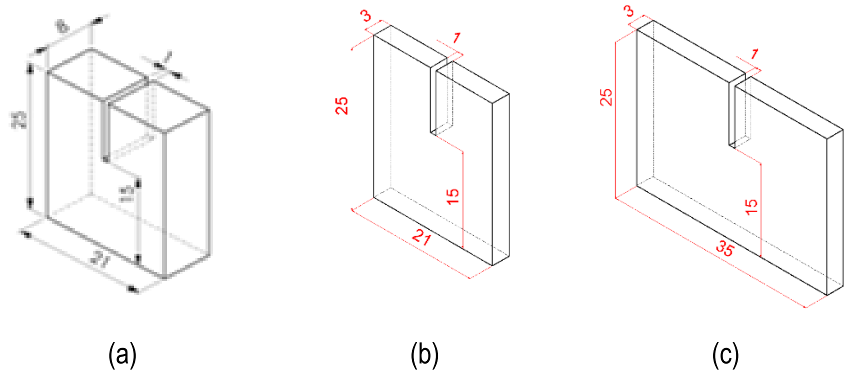

).

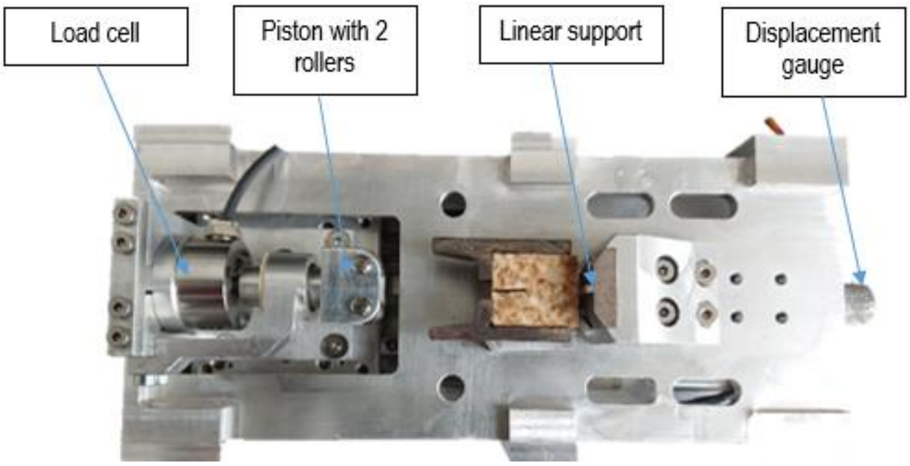

Figure 2: Miniaturized wedge splitting test device developped at MUL.

The device contains a loadcell to measure the applied load, a displacement gauge to measure the displacement, a piston with two rollers to apply vertical force on the steel adapters and a linear support to facilitate the sample deformation and the crack initiation. From the raw data, which consists of applied load and displacement, the specific fracture energy and the nominal notch tensile strength can be evaluated using (equ. 1 and (equ. 2 respectively [4].

$$G_f' = \frac{1}{A}\int_0^{\delta F_{H,15\%\,\max}} F_H . d\delta \qquad \text{(equ. 1)}$$

$$\sigma_{NT} = \frac{F_{H,max}}{b.h}\left(1 + \frac{6.y}{h}\right) \qquad \text{(equ. 2)}$$

Initially, the sample's old geometry was 25x21x8 mm³. As initial results showed no direct influence of bigger grains in the crack path on the shape of the load/displacement curve, the thickness of the sample was reduced from 8mm to 3mm. This reduction in thickness would allow a better correlation of the observed crack propagation with the corresponding load/displacement curve as the maximum grain size could vary from 1 to 3 mm. Nevertheless, the very first results obtained from this second tested geometry, exhibited an inadequate propagation of the crack that mainly was taking place between the notch and the side of the sample (Figure 3).

Figure 3: Crack propagated to the side of samples with reduced thickness.

A solution for this problem was to increase the width of the sample from 25mm to 35 mm, thus allowing the crack to propagate in designated fracture zone located under the notch. Finally, the retained new suitable geometry of the sample is today 25x35x3 mm³ (Figure 4).

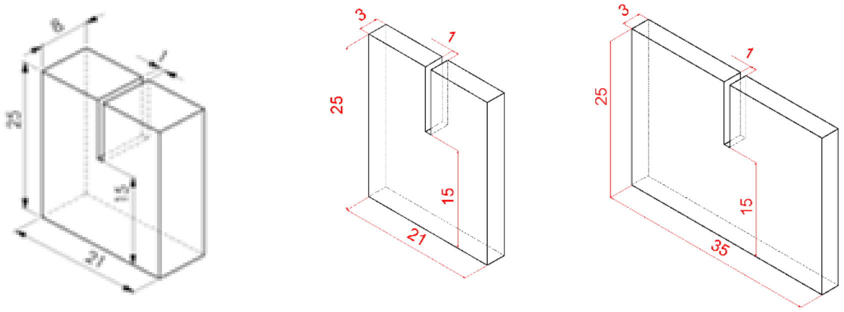

(a) (b) (c)

Figure 4: Sample geometries, (a) old geometry, (b) reduced thickness geometry, (c) new geometry.

2.2 Device developped at UNILIM

The mini wedge splitting device, developed in the University of Limoges, was originally a microtest device from DEBEN, designed for tensile and compression test in SEM (Figure 5: DEBEN Microtest device at UNILIM.). The dimensions are about 150x120x40 mm³.

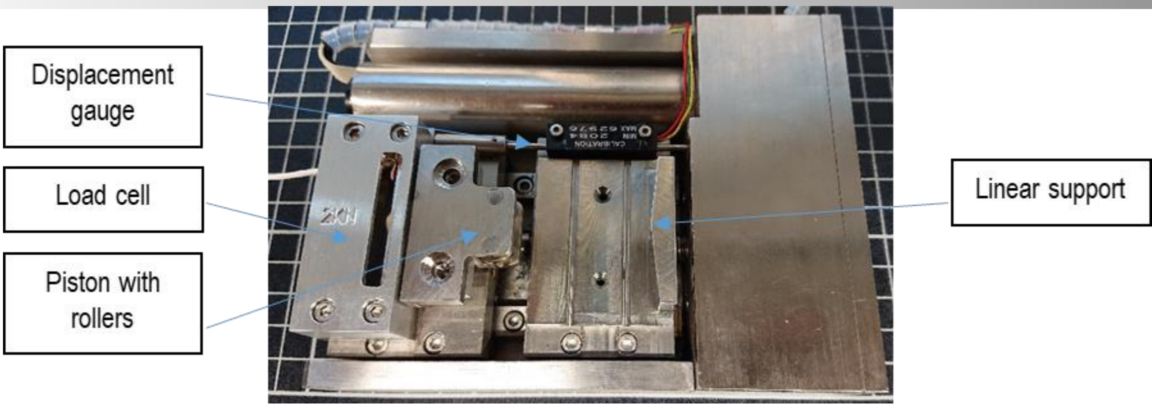

Figure 5: DEBEN Microtest device at UNILIM.

Several parts were manufactured specifically for the miniaturized wedge splitting test. Figure 6 shows the parts used to enable the adaption of the DEBEN device, such as piston with rollers and sample platform with linear support. The loadcell of this device offers different capacities (66 N, 2000 N and 5000 N), which makes testing of materials such as alumina spinel castables possible.

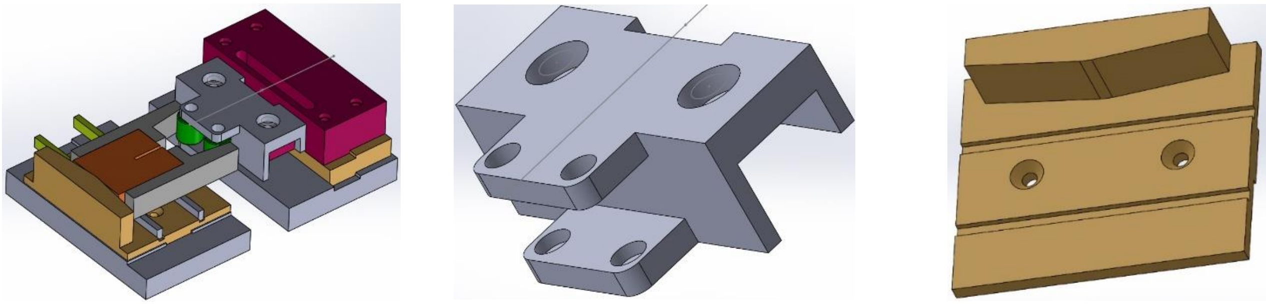

(a) (b) (c)

Figure 6: Specific parts developed for the miniaturized wedge splitting test device in the University of Limoges: (a) assembled view, (b) piston, (c) sample platform with linear support.

3 Results obtained on alumina spinel refractory bricks

3.1 Description of investigated alumina spinel materials

Alumina spinel refractory bricks are used in the working linings of the steel ladle and is composed of 94% Al_2O_3, 5% MgO, 0.3% SiO_2, and 0.1% Fe_2O_3. The spinel was introduced to the material in order to increase the corrosion resistance and potentially reduce the brittleness of the brick. To carry out mini wedge splitting tests, samples with dimensions of 25x21x8 mm^3 first, and finally 25x35x3 mm^3, were glued to two steel adapters. The test was then performed at room temperature, and the fracture was observed with an optical microscope.

3.2 Summary of results

The results obtained for alumina spinel samples, with the dimensions of 25x21x8 mm^3 and 25x35x3 mm^3, are shown in Figure 7 and Figure 8 respectively.

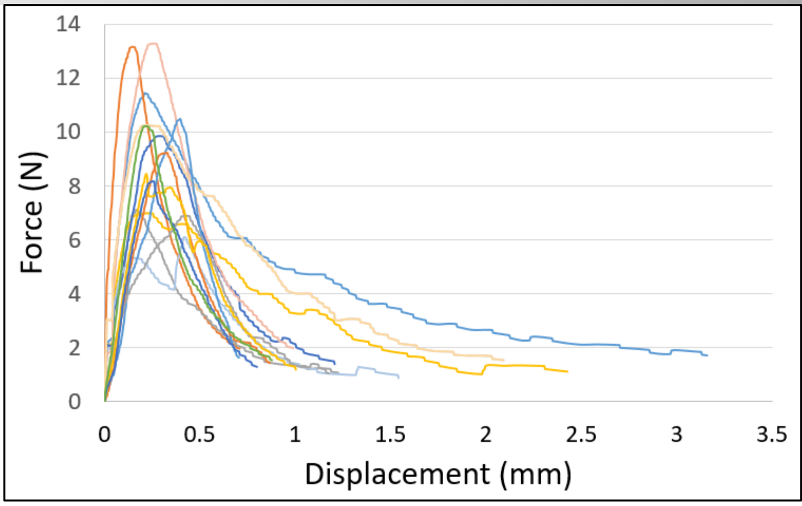

Figure 7: Summary of results from alumina spinel samples with old geometry (25x21x8 mm³).

The maximum load for alumina spinel samples with the first tested geometry range from 5.5 N to 13 N. The maximum displacement (the load required to reach 15% of the maximum load) ranges from 1.2 mm to 3.2 mm and it is within the expected range. The form of all the load/displacement curves have rather similar shape, i.e. a peak load at around 0.25 mm displacement followed by a gradual decrease in the load. Nonetheless, due to the heterogeneous microstructure of this material the maximum load and displacement of each curve varies widely. The microcracks generated by the spinel formation support the heterogeneity.

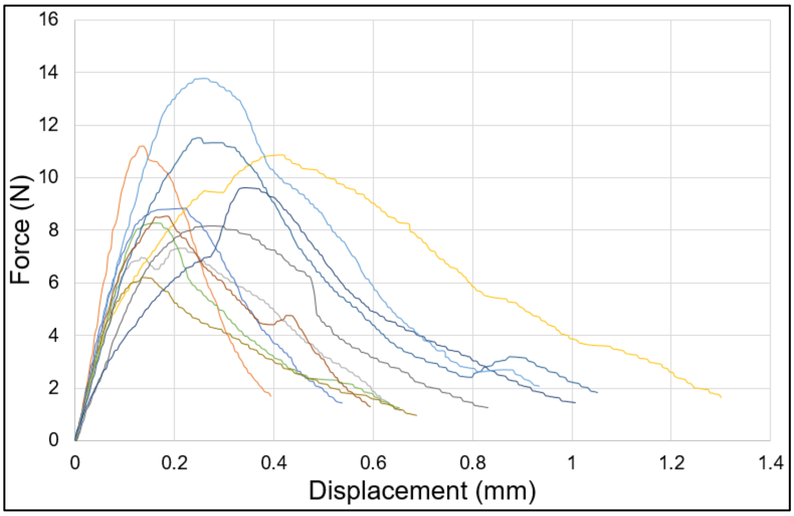

Figure 8: Summary of results from alumina spinel samples with new geometry (25x35x3 mm³)

The maximum load for alumina spinel samples, with the new geometry, range from 6 N to 14 N. The maximum displacement (the load required to reach 15% of the maximum load) ranges from 0.4 mm to 1.3 mm. The load/displacement curves do not follow a fixed trend, the peak loads range from 0.1 mm to 0.4 mm displacement followed by a gradual decrease in the load. This could be due to the reduction of the sample's thickness which increases the influence of local heterogeneities.

The average maximum load, the average specific fracture energy and the average notch tensile strength were then evaluated and gathered in Table 1. The average maximum load for the old geometry is less than for the new geometry, although the samples with old geometry lead to a more important average specific fracture energy. The average notch tensile strength is higher for the old geometry.

Table 1: Synthesis of the results from alumina spinel samples.

Geometry	Average maximum load (N)	Average specific fracture energy (N/m)	Average notch tensile strength (MPa)
Old	8.99	0.03	1.1
New	9.47	0.01	0.8

European Commission
Horizon 2020 European Union funding for Research & Innovation

Initial observations of the crack propagation, via an optical microscope, showed that samples from alumina spinel bricks favour crack propagation within the matrix and at the interface between grains and matrix (

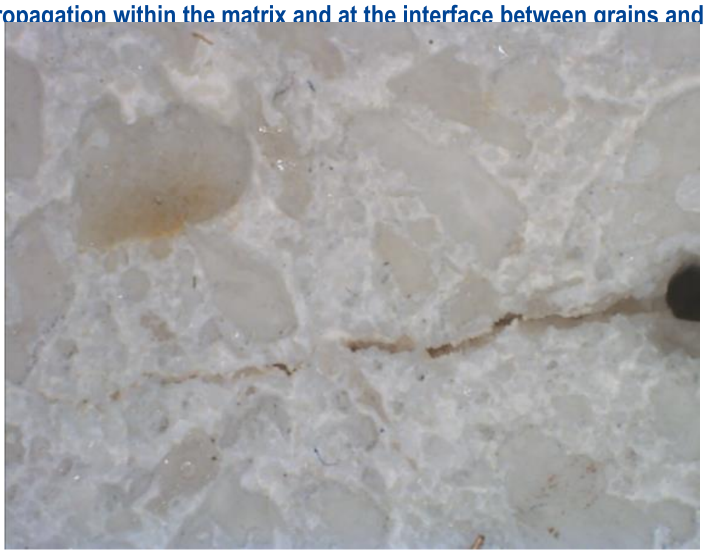

Figure 9). No transgranular crack propagation was observed as the local strength required to break the bond between grains and matrix, is significantly lower than the local strength required to break a grain. This has already been reported by Harmuth *et al.*(2010) [4].

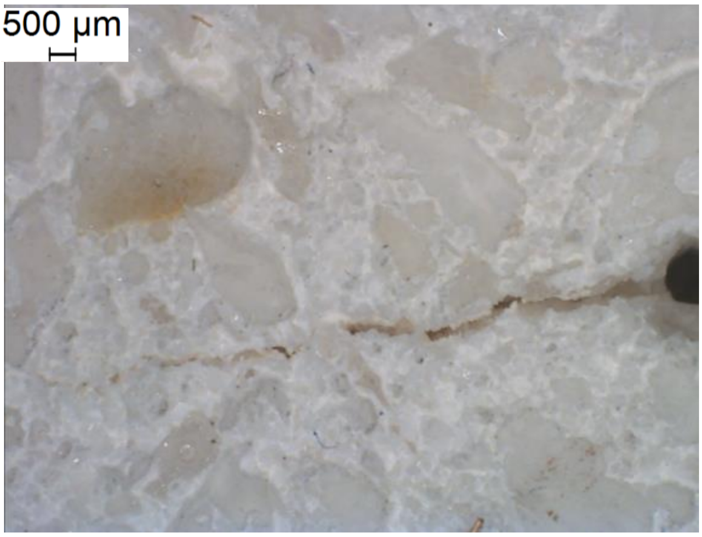

Figure 9: Example of a crack propagation within an alumina spinel sample.

4 Results obtained on magnesia spinel refractory bricks

4.1 Description of investigated magnesia spinel materials

Shaped magnesia spinel refractory bricks are composed of 87.9% MgO, 10.5% Al_2O_3, 0.5% Fe_2O_3, 0.8% CaO and 0.3% SiO_2. To carry out mini wedge splitting tests, samples with dimensions of 25x21x8 mm^3 and 25x35x3 mm^3, were glued to two steel adapters. The test was performed at room temperature and the fracture process was observed with an optical microscope.

4.2 Summary of results

The results from miniaturized wedge splitting test with magnesia spinel samples with the dimensions of 25x21x8 mm^3 and 25x35x3 mm^3, are shown in Figure 10 and Figure 11, respectively.

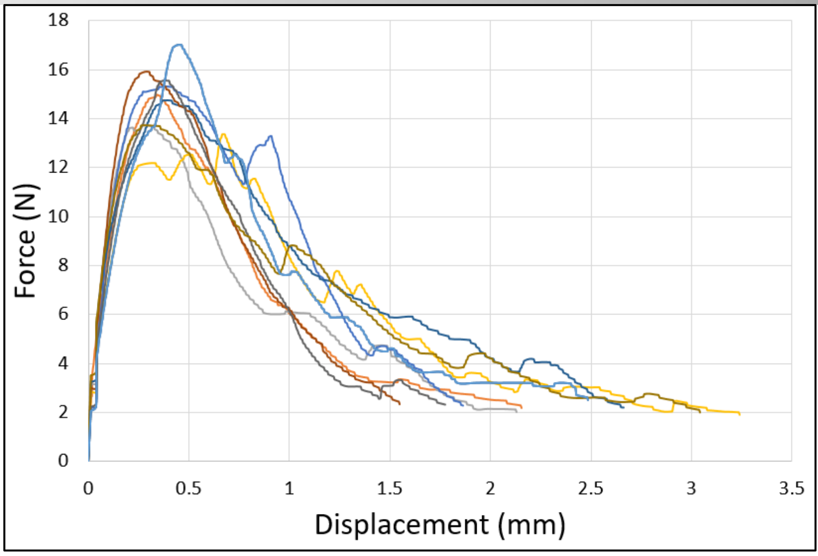

Figure 10: Summary of results from magnesia spinel samples with old geometry (25x21x8 mm³).

The maximum load for magnesia spinel samples, with the old geometry, range from 12 N to 17 N. The maximum displacement (the load required to reach 15% of the maximum load) ranges from 1.5 mm to 3.2 mm and it is within the expected range. The shape of all the load/displacement curves follow a same trend and are quite uniform, with a peak load at around 0.4 mm displacement followed by a gradual decrease in the load. Although some sudden load increases can be observed within the second part of the curves.

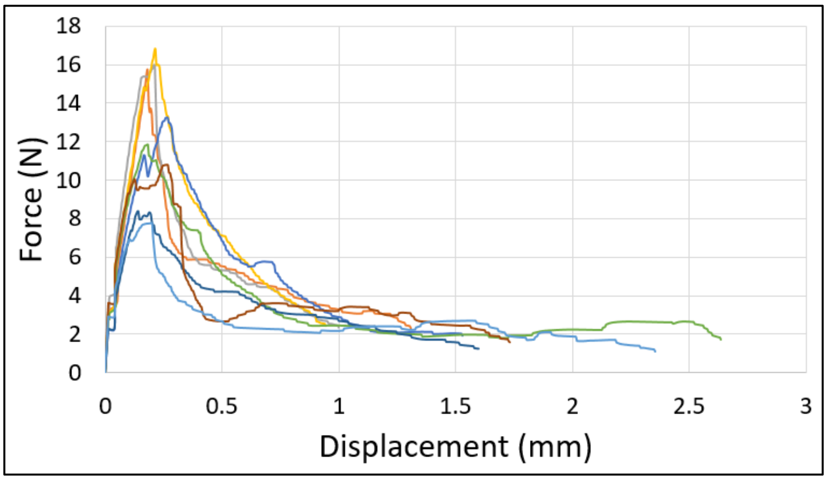

Figure 11: Summary of results from magnesia spinel samples with new geometry (25x35x3 mm³).

The maximum load for magnesia spinel samples, with the new geometry, ranges from 8 N to 16 N. The maximum displacement (the load required to reach 15% of the maximum load) ranges from 1.5 mm to 2.6 mm. Similar to the old geometry, the shape of all the load/displacement curves follow rather the same trend, with a peak load at around 0.2 mm displacement followed by a gradual decrease in the load. The reduction of the sample's thickness decreases the maximum load as well as the maximum displacement.

Table 2 shows the average maximum load, average specific fracture energy and the average notch tensile strength for magnesia spinel samples. The average maximum load with the old geometry is higher than that with the new geometry, and the required average specific fracture energy is higher with the old geometry. The average notch tensile strength follows the same trend.

Table 2: Synthesis of the results from magnesia spinel samples.

Geometry	Average maximum load (N)	Average specific fracture energy (N/m)	Average notch tensile strength (MPa)
Old	14.75	0.04	1.8
New	12.36	0.02	1.4

An example of crack propagation within a magnesia spinel sample can be observed in Figure 12. All results showed crack propagation within the matrix and at the interface between grains and matrix. Transgranular crack propagations were not observed as the local strength required to break the bond between the matrix and the grains, is significantly lower than that required to break the grains. In Figure 12, some grains rotations and some crack branching can be also observed. These events could explain the sudden load increases that appear sometime within the second part of the load/displacement curves.

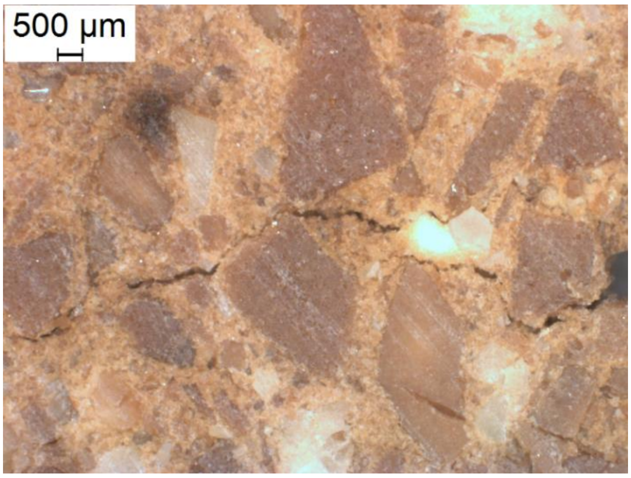

Figure 12: Example of a crack propagation within a magnesia spinel sample.

5 Results obtained from crack observation with SEM

5.1 Description of investigated materials and SEM setup

New sample geometry was used in these experiments as the old sample geometry of 8 mm thickness showed no clear evidence for the influence of single grain on the load/displacement curve. Samples were cut from magnesia, magnesia spinel, magnesia carbon and alumina spinel bricks. The sample's surface was spattered with platinum particles as it is necessary for the high vacuum mode in the SEM (Figure 13).

Figure 13: Sample's surface before and after the spattering of platinum particles.

The miniaturized wedge splitting test (MWST) device from Limoges is directly mounted on the platform of the SEM QUANTA450 from FEI. An adaptor has been installed by DEBEN to connect the MWST device to the module outside of the SEM chamber as shown in Figure 14. The SEM was set on high vacuum mode with 15 kV scanning voltage. The backscatter detector was used to monitor the crack propagation of the samples and the observation field obtained was up to 7x10 mm^2.

European Commission | Horizon 2020 European Union funding for Research & Innovation

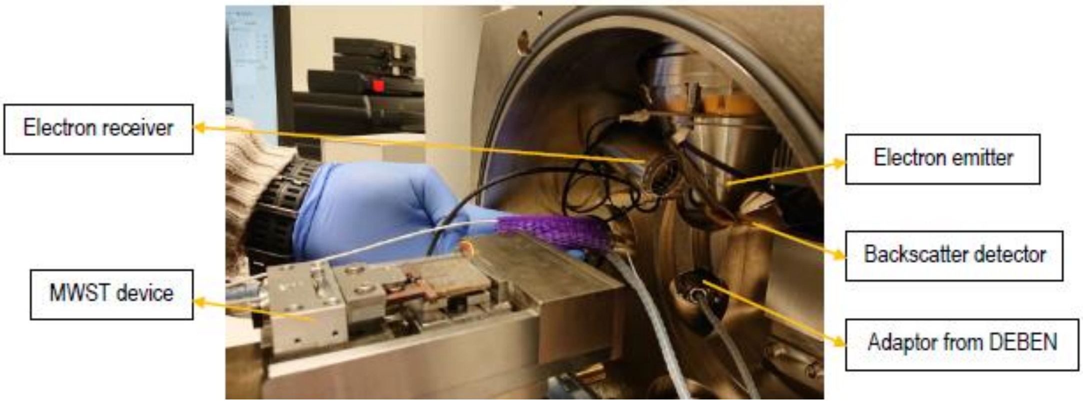

Figure 14: Miniaturized wedge splitting test with SEM setup.

5.2 Summary of results

The results from MWST with magnesia, magnesia spinel and magnesia carbon samples with SEM can be seen in

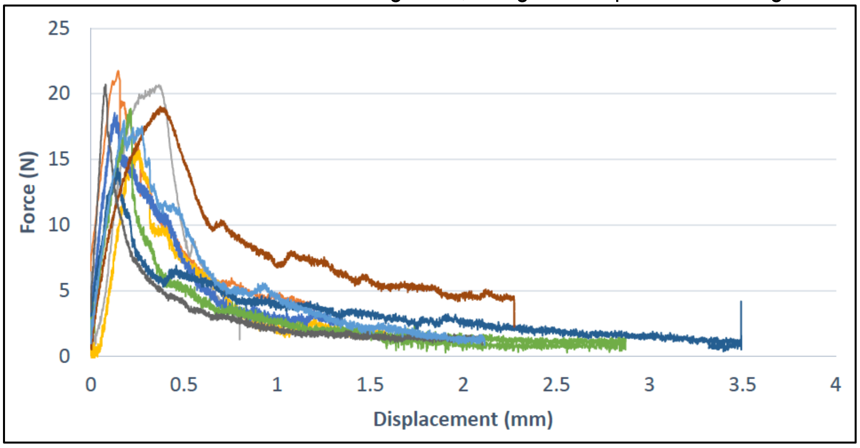

Figure 15, Figure 16 and Figure 17 respectively.

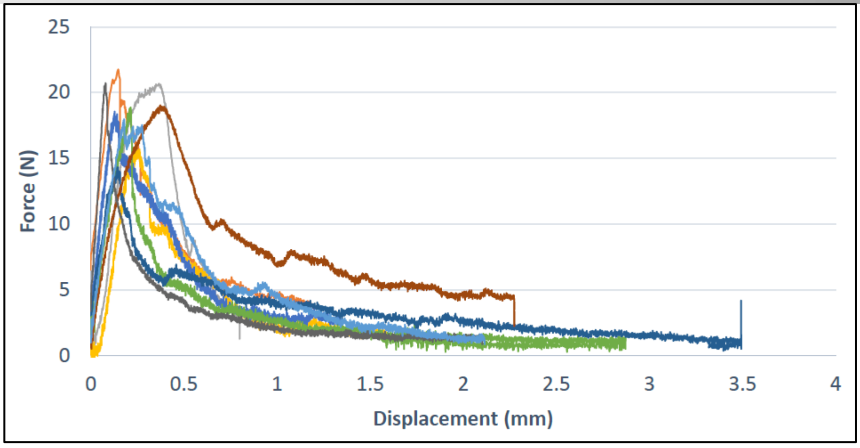

Figure 15: Summary of results from magnesia samples.

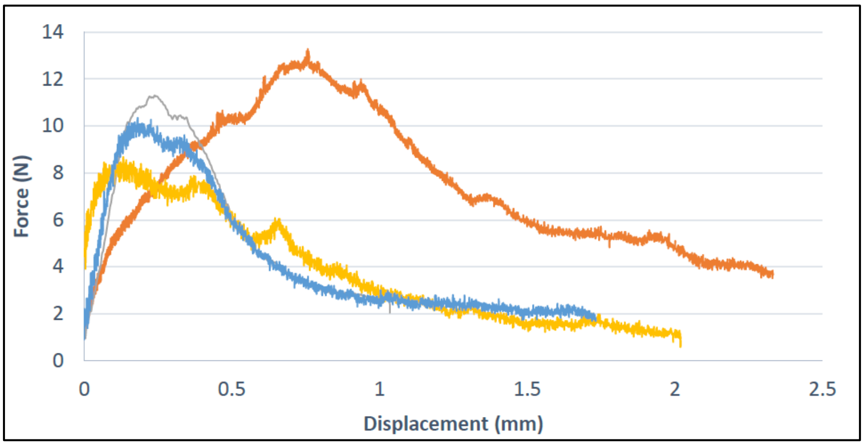

Figure 16: Summary of results from magnesia spinel samples.

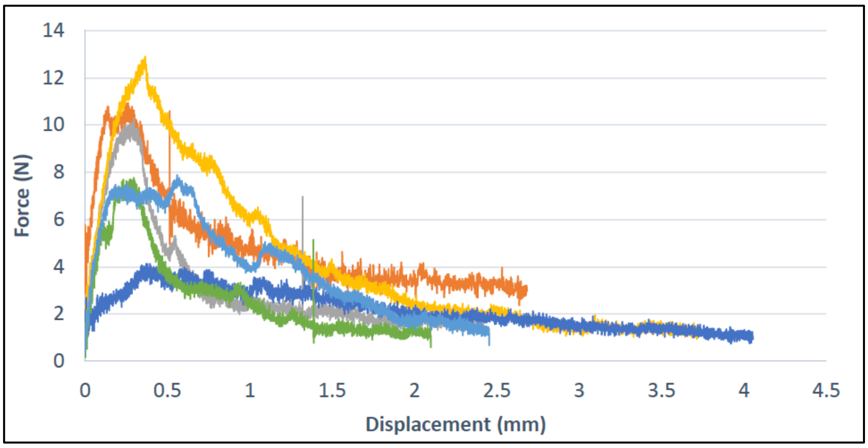

Figure 17: Summary of results from magnesia carbon samples.

The maximum load for magnesia samples ranges from 15 N to 21 N, 8 N to 12 N for magnesia spinel samples and 4 N to 13 N for magnesia carbon samples. Due to the limited space between the linear support and the piston, most of the load/displacement curve does not reach 15% of the maximum load.

Table 3 shows the average maximum load, average specific fracture energy and the average notch tensile strength for magnesia, magnesia spinel and magnesia carbon samples. The average maximum load of magnesia samples is higher than that of magnesia spinel and magnesia carbon samples although the required average specific fracture energy is higher with magnesia spinel and magnesia carbon. The average notch tensile strength follows the same trend as the average maximum load.

Table 3: Synthesis of the results from magnesia, magnesia spinel and magnesia carbon samples.

Material	Average maximum load (N)	Average specific fracture energy (N/m)	Average notch tensile strength (MPa)
Magnesia	19.9	0.05	2.1
Magnesia spinel	10.1	0.06	1.4
Magnesia carbon	9.2	0.06	1.3

Figure 18 shows a rather rare case of a crack propagation through a magnesia grain within a magnesia spinel sample. Normally the crack would avoid the grain and propagate preferably in the boundary between the grain and the matrix as seen in Figure 19 which offer a bigger view to the same crack propagation. On the left lower corner of Figure 19 is the grain shown in Figure 18. The field of observation is 0.8x1 mm² for the smaller view and 2.8x3.5 mm² for bigger view.

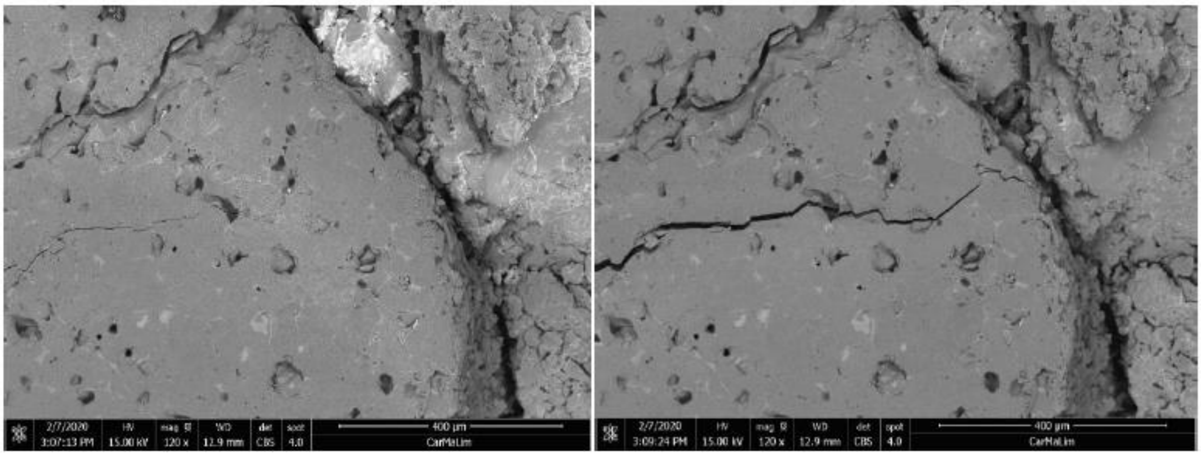

Figure 18: Smaller view of a crack propagation at different load level through a magnesia grain.

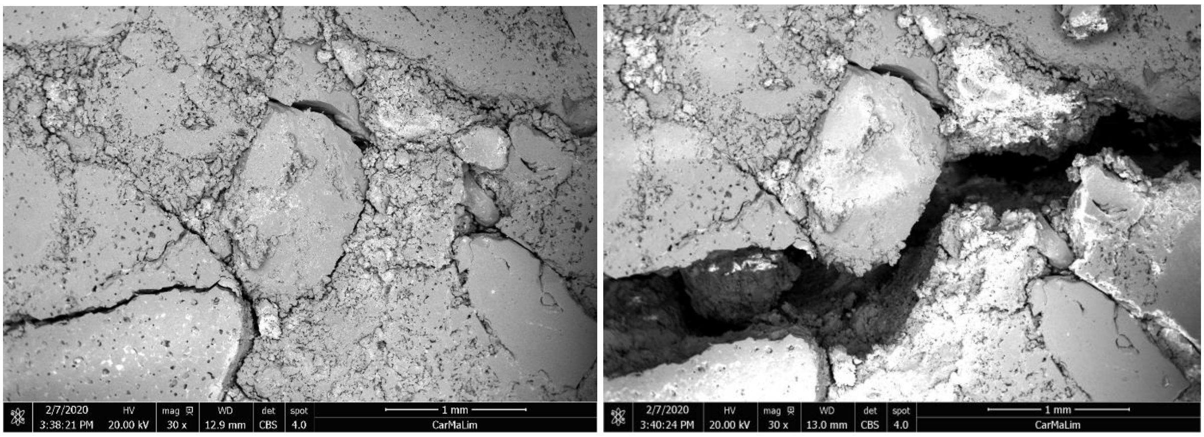

Figure 19: Bigger view of a crack propagation at different load level through a magnesia grain.

6 Results obtained from alumina spinel model refractory castables

6.1 Description of investigated alumina spinel model castables

The chosen materials for this part were six different types of model castables, cast by Saint-Gobain. The naming of these materials is following the coding logic shown in Figure 20.

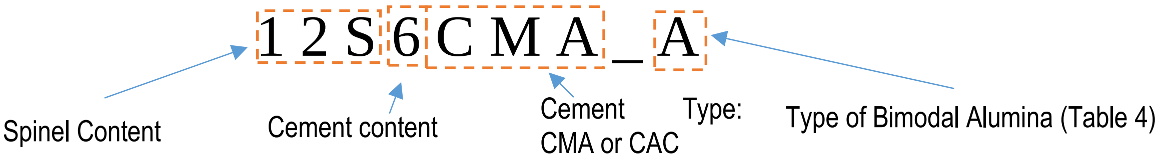

Figure 20: Coding of the name of castables.

The composition of these six different castables is shown in Table 4 and Table 5.

Table 4: The composition of the tested castables.

Raw-materials	Size	Compositions / content (wt%)					
		12S6CMA_A	12S6CAC	6S12CMA_A	6S12CMA_B	6S12CMA_C	6S12CMA-WFA
	Variant	Tabular	Tabular	Tabular	Tabular	Tabular	White Fused
Tabular Alumina	6-3 mm	23	23	23	23	23	
Tabular Alumina	3-1 mm	10	10	10	10	10	
Tabular Alumina	1-0.5 mm	19	19	19	19	19	
Tabular Alumina	0.5-0.0 mm	24	24	24	24	24	
White Fused Alumina	6-3 mm						23
White Fused Alumina	3-1 mm						10
White Fused Alumina	1-0.5 mm						19
White Fused Alumina	0.5-0.0 mm						24
Calcined Alumina	d50=5µm	2	2	2	2	2	2
Bimodal Reactive Alumina	A	3	3	3			3
Bimodal Reactive Alumina	B				3		
Bimodal Reactive Alumina	C					3	
AR78 Spinel	< 45 µm	5	5	0	0	0	0
AR78 Spinel	< 20 µm	7	7	6	6	6	6
CMA Cement	CMA72	6	0	12	12	12	12
CAC	Secar 71	0	6	0	0	0	0
Dispering Additive	Refpac 200	1	1	1	1	1	1

Table 5: Additional information for Bimodal Reactive Alumina.

Bimodal Reactive Alumina	Soda Level	Silica Level	Fine Proportion	D10 (µm)	D50 (µm)	D90 (µm)
A	Low: 500ppm	High: 700ppm	Medium	0.4	2.5	4.8
B	Low: 500ppm	High: 700ppm	High	0.2	1.4	4.5
C	High: 2300ppm	Low: 130ppm	Medium	0.4	2.5	4.8

Table 6 shows the Calcium oxide content (CaO) of the materials. Material 12S6CAC has a higher content of CaO in comparison to the material 12S6CMA_A. The material 12S6CAC has therefore a more active cement since CaO has replaced the spinel.

Table 6: Calcium oxide content (CaO) of the materials.

Material Name	12S6CMA_A	12S6CAC	6S12CMA_A	6S12CMA_B	6S12CMA_C	6S12CMA-WFA
CaO content (%)	0.6	1.8	1.2	1.2	1.2	1.2

6.2 Summary of results

For the Mini Wedge Splitting Tests (MWST), parallelepipedic samples with the standard old dimension of 25×21×8 mm³ were prepared. The test was performed while recording the force-displacement continuously, a film (24 frames per second) was also simultaneously recorded. MWST tests have been done for all six materials with two different thermal states:

- **State 1:** After drying at 110°C for 24 hours, to be sure of the conversion of hydrates into the more stable forms.
- **State 2:** After thermal treatment up to 500°C (5°C/min rate for heating and cooling with a one-hour dwell at 500°C), to ensure that the dehydroxylation process of the sample was complete.

For each material in both thermal states, at least three tests have been performed. Due to the small size of the samples and weakness of material 12S6CMA_A (the lowest cement content, see Table 4 and Table 6), it was not possible to chop it into 8 mm thickness without crushing or damaging the sample. Hence, exceptionally, 12S6CMA_A has been tested after 500°C heat treatment only. Moreover, some of the samples of other materials were crushed during the sample preparation process. Therefore, only the stronger samples have been characterised with this test; possibly leading to some artefacts. This point should be considered while reviewing the data output.

In MWST tests, a range of strength variability can be observed, even with the same tested material in the same state. This variation is due to differences in the microstructures of the different samples, especially in front of the notch. For example, as shown in Figure 21(a) for the dried state of material 6S12CMA_C, in one of the prepared samples (sample 3, in red), the notch was drilled through a grain, and the crack initiated then within this grain. This is not a common phenomenon regarding microstructure observation in front of the notch. The different force-displacement curves for the three MWST tests on this material in this same dried state are plotted in Figure 21(b). Interestingly, the force-displacement curve of the test for which the notch had been drilled through the grain, is tangibly higher than that of the other tests. This point clearly demonstrates the importance of the local microstructure in front of the notch.

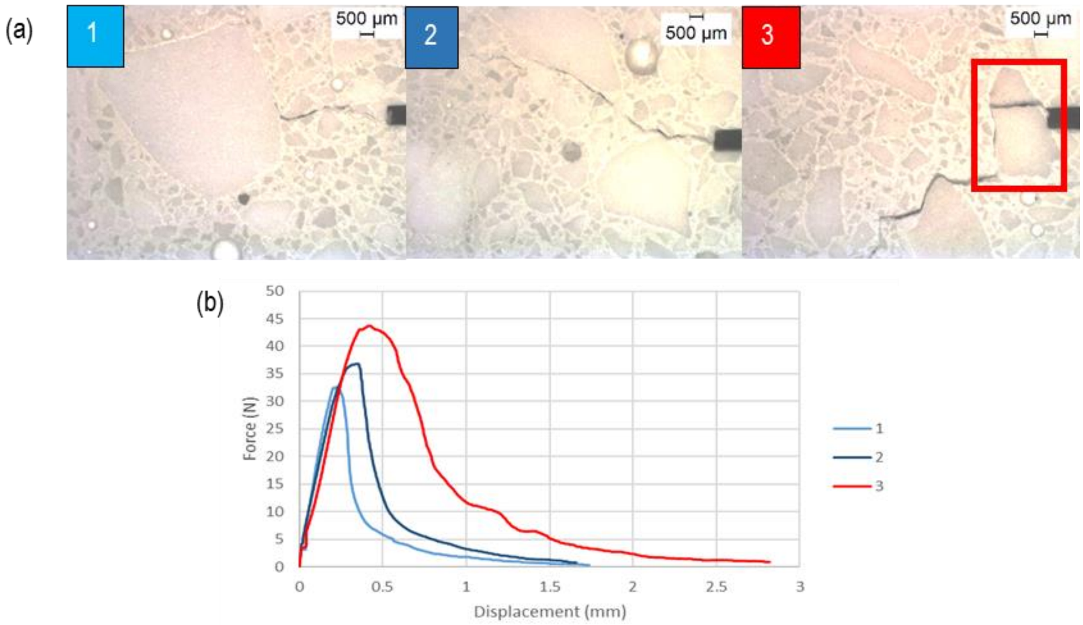

Figure 21: MWST results on three samples of a same model castable (6S12CMA_C) in dried state, (a) Microstructure observation in front of the notch, (b) Corresponding Force – Displacement curves.

The mentioned dispersion in the force-displacement curves (which is due to the different local microstructures in front of the notch), can also be seen in Figure 22. All the force-displacement curves for these tests (three tests per material per state) have been plotted: dried states curves are in the green spectrum, and curves after the 500°C thermal treatment are in the red spectrum.

European Commission
Horizon 2020
European Union funding
for Research & Innovation

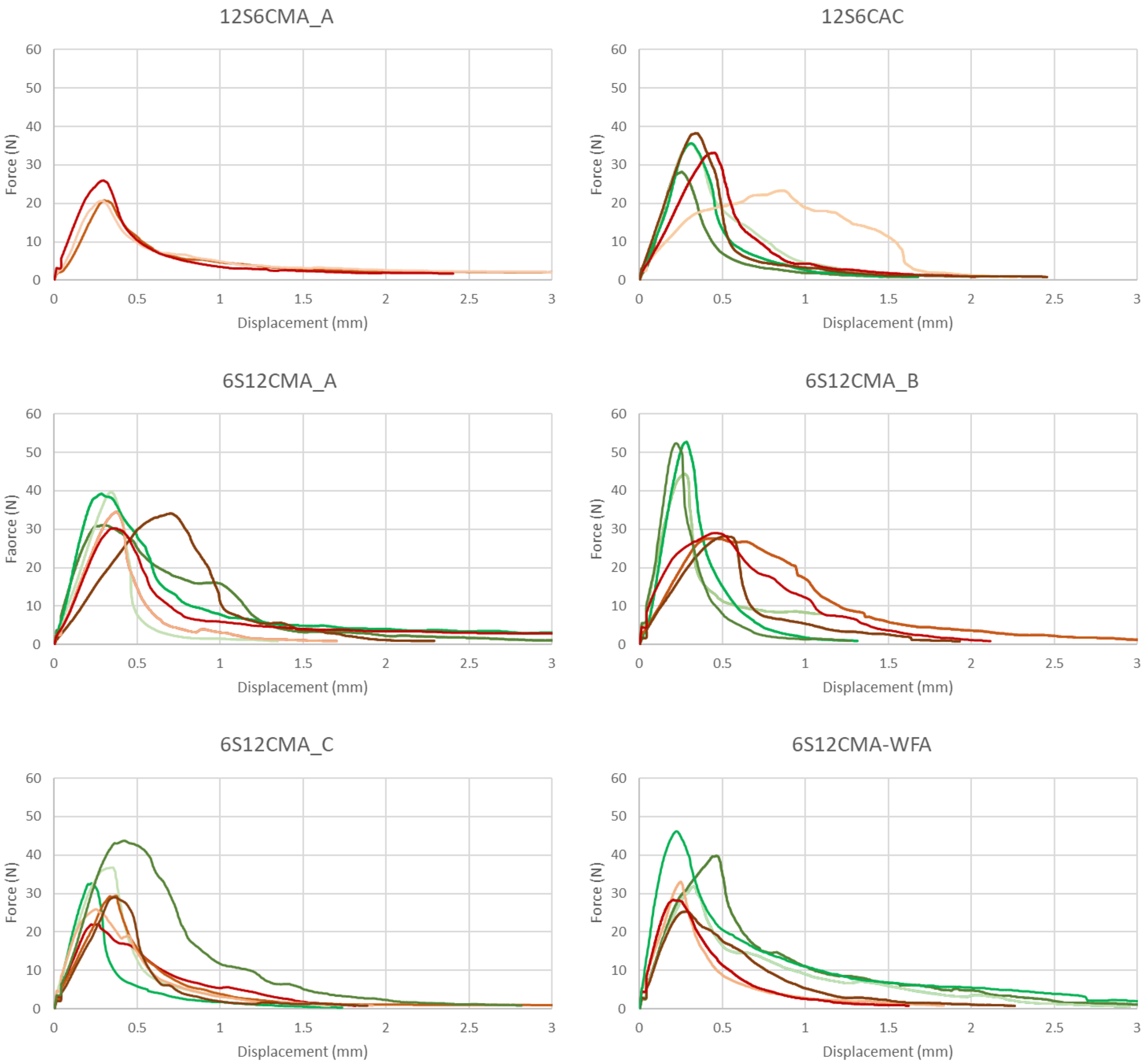

Figure 22: Force - Displacement curves during MWST for the six model castables,
dried states curves in the green spectrum, and curves after the 500°C thermal treatment in the red spectrum.

As shown in Figure 23, for some castables, the difference of the force-displacement curves in the dried state and after the thermally treatment is evident, such as material 6S12CMA_B, and 6S12CMA-WFA. Even though this difference is less evident for other materials, a reduction in the strength after the 500°C thermal treatment can be seen with all the materials.

To have a better overview, the median curve of each test set was chosen as a representative to compare the force-displacement curve of the materials in the two states: After drying at 110°C (in green) and after thermal treatment at 500°C (in red), as shown in Figure 22. As can be seen, as a general behaviour of all materials, the peak value of the force-displacement curve decreased after the thermal treatment.

Beside each material curves, the photos of the samples in the final stage of the test has been shown in Figure 23. They are showing the crack propagation among the microstructure of the samples, both in dried and thermally treated states.

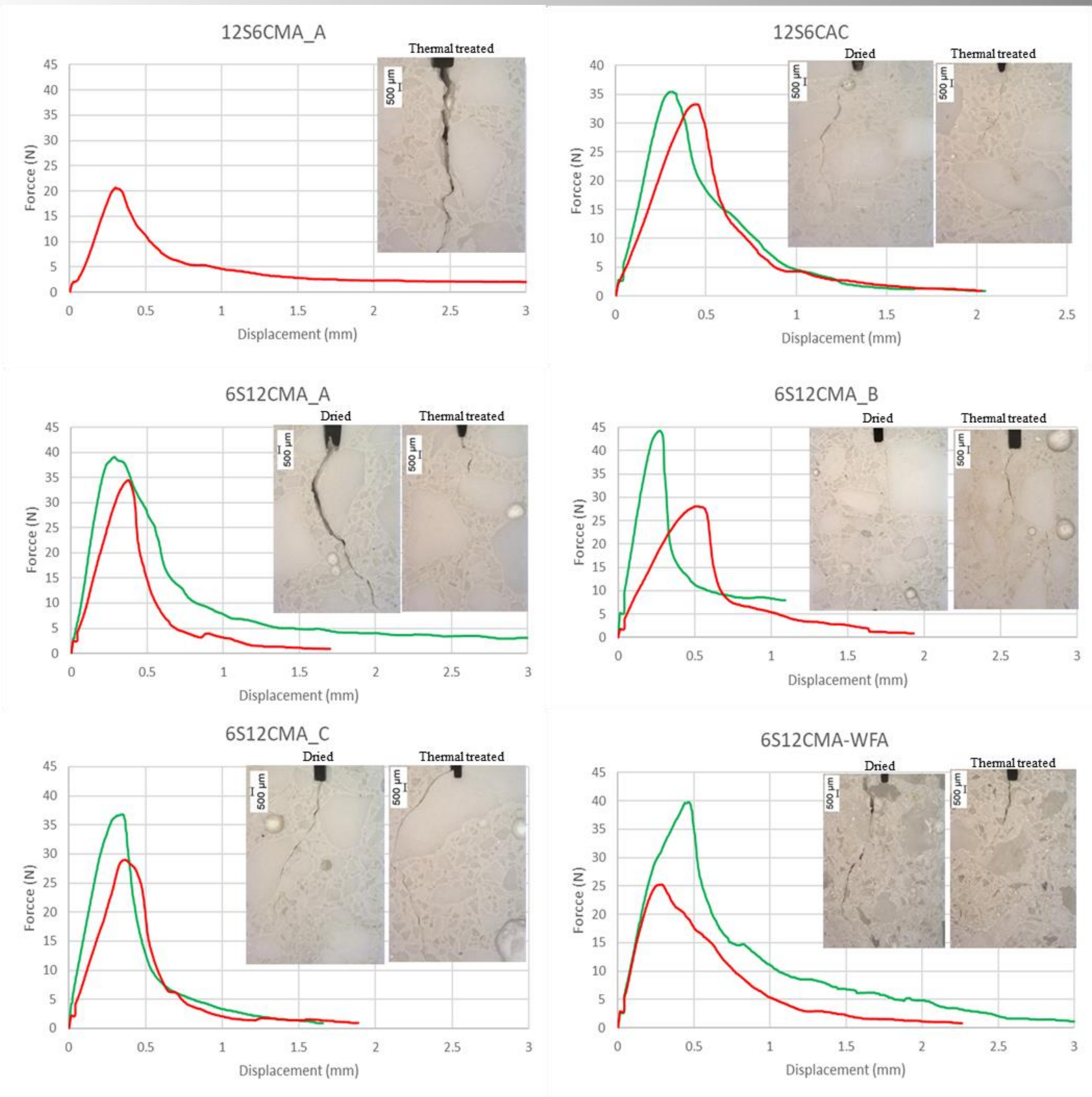

Figure 23: Force - Displacement curves during MWST for the six model castables, dried states curves in green and curves after the 500°C thermal treatment in red

Due to the lower value of the brittleness number in the dried state, more crack branching was expected to be observed in the WST results. However, the visual results did not show an evident increase in crack branching or diffused damages before and after heat treatment.

7 Conclusion

The wedge splitting test (WST) is today a standard experimental method that allow to quantify specific fracture energy and brittleness number of refractory materials. In order to comfort the interpretation of the WST results with microstructural aspects of the investigated materials, it could be very useful now to in situ monitor crack propagation through the microstructure at the surface of the samples during loading. Nevertheless, the sample size used for classical WST impedes such in situ direct observation within the limited chamber of a SEM. In order to overcome this difficulty, the purpose of the miniaturized wedge splitting test (MWST) is thus specifically to allow direct observation of crack path during loading of samples smaller enough to be in situ investigated by SEM (or optical microscopy). Such MWST devices are currently under development, one in Leoben and one in Limoges. This report reviews first results obtained on different refractory materials with these two dedicated devices.

In term of experimental development, different geometries of sample have been considered. Firstly, a sample geometry of 25x21x8 mm^3 (old geometry) was initially considered. In order to facilitate the interpretation of the load/displacement curve with the crack path progression observed in situ through the microstructure at the surface of the sample, it has been later decided to reduce the thickness of the sample from 8 mm to 3 mm. The retained new suitable geometry of the sample for this MWST is thus today 25x35x3 mm^3.

As first obtained results on all investigated materials, the form of the load/displacement curve exhibits a first part during which the load increases up to a peak (between few N and 50 N). This load peak (corresponding to a displacement between 0.1 mm and 0.5 mm) is then followed by a gradual decrease in the load. The maximum displacement (required to decrease the load down to 15% of the maximum load) ranges typically from 1 mm to 3 mm.

In the case of alumina spinel and magnesia spinel bricks, all results showed crack propagation within the matrix and at the interface between grains and matrix, but rarely in the grains. Some grains rotations and some crack branching have been also observed. These events could explain the sudden load increases that appear sometime within the second part of the load/displacement curves.

In the case of results obtained from the experiments within SEM, most of the load/displacement curve does not reach 15% of the maximum load. This is due to the limited space between the linear support and the piston. One solution to this problem is to modify the sample geometry from 25x35x3 mm^3 to 23x35x3 mm^3, and the notch length from 10 mm to 9 mm. This will slightly change the fracture zone (15x3 mm^2 to 14x3 mm^2) but the results will most probably be comparable to all results already obtained.

Regarding the results obtained on alumina spinel model refractory castables, as a general behaviour of these materials, the peak value of the force-displacement curve decreased after thermal treatment at 500°C. Different local microstructures, particularly in relation to the notch, led to dispersion in the force-displacement curves.

All these experimental results will support Discreet Element Modelling (ATHOR-WP3) and will help to build a better understanding of the relationship between the design of the microstructure of refractories and the ability of the materials to develop a R-Curve behaviour.

8 References

[1] H. Harmuth and E. K. Tschegg, 'A Fracture Mechanics Approach for the Development of Refractory Materials with Reduced Brittleness', *Fatigue Fract. Eng. Mater. Struct.*, vol. 20, no. 11, pp. 1585–1603, 1997, doi: 10.1111/j.1460-2695.1997.tb01513.x.

[2] E. K. Tschegg, K. T. Fendt, Ch. Manhart, and H. Harmuth, 'Uniaxial and biaxial fracture behaviour of refractory materials', *Eng. Fract. Mech.*, vol. 76, no. 14, pp. 2249–2259, Sep. 2009, doi: 10.1016/j.engfracmech.2009.07.011.

[3] Y. Dai, D. Gruber, and H. Harmuth, 'Observation and quantification of the fracture process zone for two magnesia refractories with different brittleness', *J. Eur. Ceram. Soc.*, vol. 37, no. 6, pp. 2521–2529, Jun. 2017, doi: 10.1016/j.jeurceramsoc.2017.02.005.

[4] H. Harmuth and R. Bradt, 'Investigation of Refractory Brittleness by Fracture Mechanical and Fractographic Methods | Fracture | Fracture Mechanics', in *Refractories manual*, 2010.

European Commission | Horizon 2020 European Union funding for Research & Innovation